Japanese Journal of Radiology
https://doi.org/10.1007/s11604-023-01445-8

ORIGINAL ARTICLE

Radioproteomics modeling of metformin-enhanced radiosensitivity: an animal study

Mohsen Cheki[1,2] · Shayan Mostafaei[3] · Mohammad Ghasem Hanafi[4] · Maryam Farasat[4] · Abdolhassan Talaiezadeh[1] · Mohammad Sadegh Ghasemi[1] · Mohammad Modava[5] · Hamid Abdollahi[6,7]

Received: 13 January 2023 / Accepted: 8 May 2023

Abstract

Purpose Metformin is considered as radiation modulator in both tumors and healthy tissues. Radiomics has the potential to decode biological mechanisms of radiotherapy response. The aim of this study was to apply radiomics analysis in metformin-induced radiosensitivity and finding radioproteomics associations of computed tomography (CT) imaging features and proteins involved in metformin radiosensitivity signaling pathways.

Materials and methods A total of 32 female BALB/c mice were used in this study and were subjected to injection of breast cancer cells. When tumors reached a mean volume of 150 mm^3, mice were randomly divided into the four groups including Control, Metformin, Radiation, and Radiation + Metformin. Western blot analysis was performed after treatment to measure expression of proteins including AMPK-alpha, phospho-AMPK-alpha (Thr172), mTOR, phospho-mTOR (Ser2448), phospho-4EBP1 (Thr37/46), phospho-ACC (Ser79), and β-actin. CT imaging was performed before treatment and at the end of treatment in all groups. Radiomics features extracted from segmented tumors were selected using Elastic-net regression and were assessed in terms of correlation with expression of the proteins.

Results It was observed that proteins including phospho-mTOR, phospho-4EBP1, and mTOR had positive correlations with changes in tumor volumes in days 28, 24, 20, 16, and 12, while tumor volume changes at these days had negative correlations with AMPK-alpha, phospho-AMPK-alpha, and phospho-ACC proteins. Furthermore, median feature had a positive correlation with AMPK-alpha, phospho-ACC, and phospho-AMPK-alpha proteins. Also, Cluster shade feature had positive correlations with mTOR and p-mTOR. On the other hand, LGLZE feature had negative correlations with AMPK-alpha and phospho-AMPK-alpha.

Conclusion Radiomics features can decode proteins that involved in response to metformin and radiation, although further studies are warranted to investigate the optimal way to integrate radiomics into biological experiments.

Keywords Metformin · Radiation · Radiomics · Proteomics · Computed tomography

✉ Mohsen Cheki
mohsencheky@gmail.com

✉ Hamid Abdollahi
habdollahi@bccrc.ca

[1] Cancer Research Center, Ahvaz Jundishapur University of Medical Sciences, Ahvaz, Iran

[2] Department of Medical Imaging and Radiation Sciences, Faculty of Paramedicine, Ahvaz Jundishapur University of Medical Sciences, Ahvaz, Iran

[3] Department of Medical Epidemiology and Biostatistics, Karolinska Institutet, Stockholm, Sweden

[4] Department of Radiology, Ahvaz Jundishapur University of Medical Sciences, Ahvaz, Iran

[5] Department of Electrical Engineering, Faculty of Engineering, Shahid Chamran University of Ahvaz, Ahvaz, Iran

[6] Department of Radiology Technology, Faculty of Allied Medical Sciences, Kerman University of Medical Sciences, Kerman, Iran

[7] Department of Integrative Oncology, BC Cancer Research Institute, Vancouver, BC, Canada

Published online: 19 May 2023

Introduction

Metformin, an antidiabetic agent, was studied as a radiation modifier that acts on both normal tissues and tumors [1]. Studies have indicated that metformin can protect normal tissues against and sensitize tumors to ionizing radiation because of its interesting properties [2, 3]. The beneficial effects of metformin on radiotherapy outcomes for both cancerous and normal organs were addressed in several clinical trials [4, 5]. In an interesting review, Chevalier et al. [6], named the metformin "best friend of the radiation oncologists" and summarized the clinical benefits of metformin and its radiosensitizing mechanisms. Recently, in a systematic review, Clifford et al. [7] reviewed studies on metformin-induced radiosensitivity in pelvic malignancies. There is also a wealth of data available on the use of metformin as a feasible cellular radioprotector [8, 9].

It is revealed that metformin acts as a radiation modifier via altering some mechanisms including tumor hypoxia, intrinsic radiosensitivity, tumor proliferation rates, and fraction of tumor stem cells [10, 11]. The radiosensitizing mechanisms of metformin were investigated by several studies and main biological pathways were identified. One of the main genetic approach that mediates metformin's modulation of radiation response is adenosine monophosphate activated kinase (AMPK) signaling pathway [12]. AMPK acts via phosphorylation and inactivation of acetyl coenzyme A carboxylase (ACC). AMPK also phosphorylates some proteins to inhibit mammalian target of rapamycin (mTOR) signaling [13]. The mTOR kinase by phosphorylation of regulators such as eukaryotic translation initiation factor 4E-binding protein (4EBP1) regulates cellular metabolism, growth, and proliferation [14].

Recently, many attempts have been made to find biological pathways involved in cancer diagnosis and treatment using quantitative parameters extracted from medical images [15, 16]. Several studies have identified that radiomics features could predict the mutation status of different genes that have roles in cancer diagnosis and prognosis, specific molecular pathways in cancer development, and the immunological mechanisms of cancers [17]. Furthermore, radiogenomics studies have revealed that several imaging features have correlations with genes or proteins that play role in cancer biology [18].

Although, most radiomics studies have been conducted in the clinic and with human data, several research works were performed in the laboratory and on animals [19]. In animal radiomics studies, researchers enable better understanding of the biological meaning of radiomics and also examine different therapeutics to find most individualized treatment for several diseases [20]. In another way, because metformin was known as a radiation modifier that could enhance the radiosensitivity of tumors via activating some signaling pathways, modeling the radiosensitivity of such agents will provide more accurate selecting patients/radiosensitizers and decoding the signaling pathways in the road of personalized medicine. This study aims to apply radiomics analysis for metformin-induced radiosensitivity and finding radioproteomics associations between computed tomography (CT) imaging features and proteins involved in metformin radiosensitivity signaling pathways.

Materials and methods

Animals

A total of 32 female BALB/c mice, 6–8 weeks of age, 20 g in weight, were used in this study. All of the mice were kept in a room under constant temperature (22 ± 2 °C), humidity (55–60%), and illuminated 8:00 a.m. to 8:00 p.m. The animals were accustomed to the laboratory conditions for a week prior to the experimentation session.

Experimental design and treatment protocol

Subcutaneous tumors were established by injecting 1×10^6 4T1 breast cancer cells into the right dorsal flank of BALB/C mice. When tumors reached a mean volume of 150 mm^3, mice were randomly divided into the following four groups ($n = 8$ for each group):

Control: animals were treated with drinking water containing no metformin for 4 consecutive weeks and exposed to sham irradiation on the 7th day.

Metformin: animals were treated with drinking water containing metformin (300 mg/kg body weight per day) for 4 consecutive weeks and exposed to sham irradiation on day 7.

Radiation: animals were treated with drinking water containing no metformin for 4 consecutive weeks and exposed to a single dose of 10 Gy X-rays on the 7th day.

Radiation + Metformin: animals were treated with drinking water containing metformin (300 mg/kg body weight per day) for 4 consecutive weeks and exposed to a single dose of 10 Gy X-rays on the 7th day.

Metformin was daily administered at 300 mg/kg body weight via drinking water till euthanasia [21]. To ensure the desired concentration (300 mg/kg) of metformin in drinking water, the intake of metformin and drinking water was adjusted daily. On the other hand, tumor growth was evaluated every 4 days using a caliper and tumor volume was calculated as (long diameter) × (short diameter)^2 × 0.52 [22, 23].

Irradiation

X-ray irradiation was performed using energy 6 MV from a medical linear accelerator (Elekta, Stockholm, Sweden) at a dose rate of 2 Gy/min and a source to-surface distance (SSD) of 100 cm. The tumor on the right dorsal flank locally exposed to a single dose of 10 Gy and the rest of body was shielded by a lead sheet.

Western blot analysis

At the end of treatment procedure, on day 28, mice were euthanized by CO_2 asphyxiation and their tumors were removed. Tumor tissues were mixed with RIPA lysis buffer containing protease inhibitor cocktail (MyBioSource, USA). Lysates were centrifuged and supernatant was collected. After quantified using BCA protein assay kit (Pierce, Rockford, USA), 80 µg protein was separated by 6%-12% SDS-PAGE and transferred to polyvinylidene fluoride (PVDF) membrane (Pall, NY, USA). Membranes were blocked with 5% fat-free milk in Tris-buffered saline-Tween 20 (TBST, 20 mM Tris, pH 7.6, 137 mM NaCl, and 0.1% Tween 20) for 1 h at room temperature, followed by an overnight incubation at 4 °C with primary antibodies: AMPK-alpha, phospho-AMPK-alpha (Thr172), mTOR, phospho-mTOR (Ser2448), phospho-4EBP1 (Thr37/46), phospho-ACC (Ser79), and β-actin. The β-actin protein levels were used as a control to verify equal protein loading. All antibodies were used at a dilution of 1:1000. Blots were subsequently washed three times with TBST and then incubated with the horseradish peroxidase (HRP)-conjugated secondary antibodies 1 h at room temperature. After three additional TBST washes, the band signals were detected using an enhanced chemiluminescence (ECL) kit (Amersham Biosciences, NJ, U.S.A.) according to the manufacturer's instructions. The intensity of the protein bands in the blots was determined with ImageJ software (NIH, Bethesda, MD, USA). The levels of target proteins expression were first quantitated relative to the expression of β-actin, and then normalized to the background expression in drinking water-treated mice (control).

Computed tomography (CT) imaging

CT imaging of mice was performed before treatment (baseline: tumor volume ~ 150 mm^3) and at the end of treatment (day 28) in all groups. CT imaging was performed on a 16-slice CT scanner (Somatom Definition, Siemens Medical Solutions, Germany) using an optimized mice imaging protocol: 512 × 512-pixel matrix, 0.2 mm pixel size, 80 kVp X-ray tube voltage, 60 mA tube current, 16 × 1.2 mm collimation, 5–8 mm table feed/ rotation, 0.6 s rotation time, and slice thickness of 0.6 mm.

Tumor segmentation

The volume-of-interest (VOI) segmentation was performed manually using 3D slicer software (version 4.10.2; available at: http://slicer.org/) and verified by experienced radiologist in cancer imaging (Fig. 1).

Preprocessing and feature extraction

Before feature extraction, preprocessing steps including wavelet and Laplacian of Gaussian (LOG) filters, resampling to 1 × 1 × 1 mm^3 and discretization to 64 bin (BIN64), were applied on CT images. For LOG filter, different sigma values were used to extract fine, medium, and coarse features; specifically, they ranged from 0.5 to 5 with 0.5 steps. Wavelet filtering yields 8 decompositions per level (all possible combinations of applying either a high or a low pass filter in each of the three dimensions including HHH, HHL, HLH, HLL, LHH, LHL, LLH, and LLL). Radiomics features were extracted using the PyRadiomics version (2.2.0) implementation in python (version 3.6.4). Extracted features were categorized to the different feature classes. The classes include first order statistics (19 FOS features), shape-based (16 Shape features), gray level co-occurrence matrix (24 GLCM features), gray level run length matrix (16 GLRLM features), gray level size zone matrix (16 GLSZM features), neighboring gray tone difference matrix (5 NGTDM features), and gray level dependence matrix (14 GLDM features).

Feature selection

Feature selection was done to find the features, which are related to tumor volume using Elastic-net regularized linear regression model by "glmnet" R package (version 4.1.1). The optimal tuning parameters were estimated using leave-one-out cross-validation with 1000 bootstrapping samples by "glmnetSE" R package. Elastic-net linear regression is an extension of linear regression that includes penalties to the loss or cost function. Elastic-net is a linear combination of ridge and least absolute shrinkage and selection operator (LASSO) penalties and brings both advantages penalties of

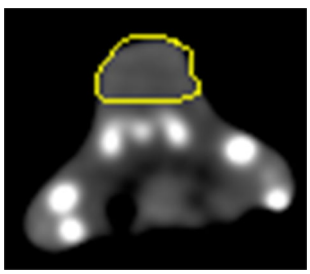

Fig. 1 Tumor delineation on axial slice of CT image

ridge and LASSO. The changes in tumor volume and radiomics features were considered as the response variable (Y) and associated features (X), respectively.

Univariate / multivariable radiomics analysis and model evaluation

To calculate *p* value for selected features in univariate and multivariable analysis, generalized linear model was applied. Also, R-squared and root mean square error (RMSE) index as goodness of fit indices for linear regression were measured to find the optimal model. Moreover, likelihood ratio test (LRT) was used for statistical comparisons between the groups. These analytical methods were performed using "glm" R function. *p* values were adjusted by Benjamini and Hochberg method [24]. We applied false discovery rate (FDR) online calculator using the web-based tool (https://www.sdmproject.com/utilities/?show=FDR). Statistical significance was considered at the level of 0.05.

Protein expression analysis and time trend analysis

After checking the parametric test assumption (e.g., normality), Kruskal–Wallis test and Dunnett's test were used for statistical comparison of the proteins expression level between studied four groups and each three intervention groups compared with control group (as a reference group), respectively. To compare time trends of tumor volume between groups over time, repeated measure ANOVA with a linear trend was used. These statistical analyses were analyzed using GraphPad Prism 6 and SPSS software (Versions 16). Statistical significance was considered at p value < 0.05.

Interactive hierarchical clustering heatmap

Hierarchical clustering heatmap plot of Spearman's correlations between proteins expression and tumor volumes and hierarchical clustering heatmap plot of Spearman's correlations between proteins expression and selected features with change tumor volume in IR plus Metformin group were drawn using "heatmaply" R package (version 4.1.1) [25].

Results

Tumor volume change

Our results on tumor volume changes in different groups based on the follow-up time are shown in Fig. 2. As was seen, the trend of tumor volume changes was significantly different among groups and the Metformin + IR group has the maximum changes after irradiation across times.

Protein expression

Our results on statistical comparisons of protein expression between each group with control as reference group are shown in Fig. 3. As shown, the expression of proteins was significantly different among different groups in comparison with control groups. Furthermore, the expression of three proteins including AMPK-alpha, phospho-AMPK-alpha, and phospho-ACC in Metformin + IR group has the highest amount in comparison with other groups, while in this group, the three remained proteins (mTOR, phospho-mTOR, and phospho-4EBP1) have the lowest values of expression.

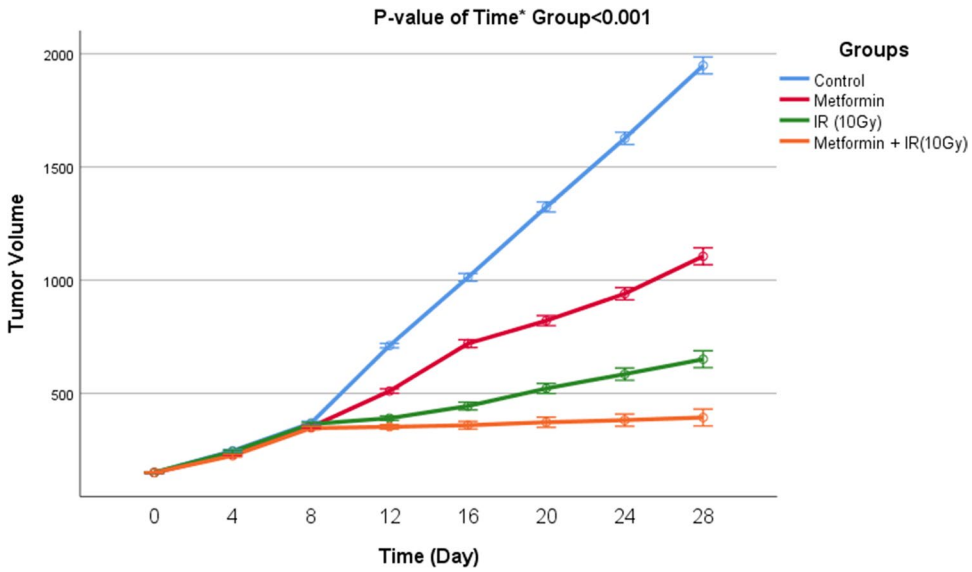

Fig. 2 Comparisons of trend curves between each three groups with control as reference group (all of p values < 0.001)

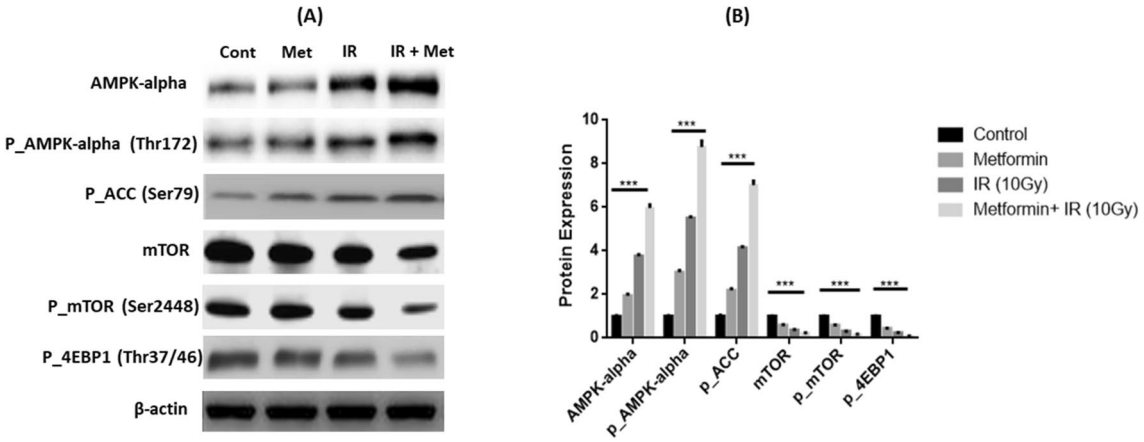

Fig. 3 Western blot analysis for the effect of metformin, 10 Gy irradiation or combined on target proteins expression level. **(A)**: shows immunoblot images of AMPK-alpha, P_AMPK-alpha (phospho-AMPK-alpha), P_ACC (phospho-ACC), mTOR, P_mTOR (phospho-mTOR), P_4EBP1 (phospho-4EBP1). β-Actin was used as loading control. **(B)**: statistical comparison of protein expression between each group with control as reference group. *** indicates significant difference between each of three groups and control group

Selected features

Our selected radiomics features to identify most related features with tumor volume at baseline are shown in Table 1. In group Control, features including wavelet-HHH_GLSZM_GLNU_Normalized, Log-Sigma-5mm_FO_Maximum, and Wavelet_HHL_GLSZM_SZNU_Normalized with, respectively, variable importance of 96%, 69%, and 64% were selected (adjusted p value < 0.05). In group Metformin, the selected radiomics features with adjusted p value < 0.05 were wavelet-LLHglrlmLongRunEmphasis, log-sigma-2–0-mm-3DglcmAutocorrelation, wavelet-LHLglrlmLongRunEmphasis, wavelet-HLLglcmSumEntropy, and wavelet-LLHglrlmGrayLevelNonUniformity. In group irradiation, features including log-sigma-1–5-mm-3Dfirstorder10Percentile and log-sigma-3–5-mm-3DglszmLargeAreaLowGrayLevelEmphasis with importance values of 97% and 58% were selected. Furthermore, in group irradiation + Metformin, radiomics features with adjusted p value < 0.05 were log-sigma-3–0-mm-3DfirstorderKurtosis, wavelet-HLLfirstorderKurtosis, log-sigma-3–5-mm-3DfirstorderKurtosis, and log-sigma-3–0-mm-3DglcmClusterShade.

Selected features to identify the most related features with tumor volume change (Day 28-baseline) are shown in Table 2. Radiomics features with adjusted p value < 0.05 in group control were wavelet-HHLglcmContrast, log-sigma-5–0-mm-3DglcmImc2, and wavelet-HLLngtdmStrength. In group Metformin, the significant features were wavelet-HHHfirstorderUniformity, log-sigma-0–5-mm-3DglrlmLongRunLowGrayLevelEmphasis, and log-sigma-3–5-mm-3DglcmInverseVariance. In group, irradiation, features including wavelet-LHLglcmInverseVariance, wavelet-HHLglszmSmallAreaLowGrayLevelEmphasis, originalglszmSmallAreaEmphasis, and wavelet-LLHglcmCorrelation were selected. In group irradiation + Metformin, selected features with adjusted p value < 0.05 were log-sigma-2–0-mm-3DglcmClusterShade, wavelet-LHHglszmLowGrayLevelZoneEmphasis, riginalgldmSmallDependenceLowGrayLevelEmphasis, wavelet-HLLgldmGrayLevelNonUniformity, wavelet-LHLngtdmStrength, log-sigma-5–0-mm-3DglcmDifferenceVariance, and wavelet-HHHfirstorderMedian.

Radioproteomics analysis

Our radioproteomics analysis is shown in Figs. 4, 5. In Fig. 4, correlation of proteins expression and tumor volume is depicted and is clearly shown that proteins including phospho-mTOR, phospho-4EBP1, and mTOR have positive correlation (more than 0.5) with changes in tumor volumes in days 28, 24, 20, 16, and 12, while tumor volume changes at these days have negative correlation with AMPK-alpha, phospho-AMPK-alpha, and phospho-ACC proteins. In Fig. 5, it is observed that some selected radiomics features have strong positive and negative correlations to selected protein expression. For example, Median feature (a first order feature) has positive correlation to proteins namely AMPK-alpha, phospho-ACC, and phospho-AMPK-alpha. Furthermore, Cluster shade (a GLCM feature) has positive correlation to mTOR and p-mTOR. On the other hand, low gray level zone emphasis (LGLZE) as a GLSZM feature has negative correlation to AMPK-alpha and phospho-AMPK-alpha.

Discussion

Metformin enhanced radiosensitivity in cancer cells and its radioprotective effect on normal cells is a promising approach to consider it as a feasible issue to increase

Table 1 Feature selection for identify of related features with tumor volume at baseline by "glmnet" and "glmnetSE" R packages with 1000 bootstrapping and leave-one-out cross-validation and "glm" R function for calculation of *p* value and comparisons among groups (control was considered as the reference)

Groups	Selected variables	Variable importance	Adj. *p* value	Adjusted R^2	*p* value of comparison between groups
Control	wavelet-HHHglszmGrayLevelNonUniformityNormalized	96%	**0.001**	0.218	Reference
	log-sigma-5–0-mm-3DfirstorderMaximum	69%	**0.028**		
	wavelet-HHLglszmSizeZoneNonUniformityNormalized	64%	**0.041**		
	wavelet-HLHfirstorderUniformity	50%	0.165		
	wavelet-LLHglcmImc2	43%	0.289		
	wavelet-HLHglcmIdmn	39%	0.714		
Metformin	wavelet-LLHglrlmLongRunEmphasis	96%	**0.001**	**0.278**	0.153
	log-sigma-2–0-mm-3DglcmAutocorrelation	69%	**0.041**		
	wavelet-LHLglrlmLongRunEmphasis	78%	**0.022**		
	log-sigma-0–5-mm-3DglcmInverseVariance	21%	0.627		
	wavelet-HLLglcmSumEntropy	79%	**0.022**		
	wavelet-LLHglrlmGrayLevelNonUniformity	87%	**0.005**		
	log-sigma-1–0-mm-3DglcmId	30%	0.468		
IR	log-sigma-1–5-mm-3Dfirstorder10Percentile	97%	**0.001**	0.229	0.768
	wavelet-HHHglcmClusterTendecy	42%	0.202		
	log-sigma-3–5-mm-3DglszmLargeAreaLowGrayLevelEmphasis	58%	**0.048**		
	log-sigma-5–0-mm-3DgldmLargeDependenceEmphasis	38%	0.354		
	wavelet-HHHglcmClusterProminence	46%	0.243		
IR + Metformin	log-sigma-3–0-mm-3DfirstorderKurtosis	79%	**0.020**	0.275	0.193
	originalngtdmContrast	36%	0.382		
	wavelet-HLLfirstorderKurtosis	60%	**0.048**		
	log-sigma-3–5-mm-3DfirstorderKurtosis	59%	**0.050**		
	log-sigma-3–0-mm-3DglcmClusterShade	71%	**0.010**		
	wavelet-LHHfirstorderMedian	55%	0.117		

p value by Wald chi-square test, Adj. *p* value: *p* value adjusted by Benjamini and Hochberg method, overall R^2 is based on the multivariable linear regression, last column indicates *p* values for statistical comparisons of the linear models among the groups (Control as a reference group) using likelihood ratio test (LRT), bold adjusted R-squared indicates the best outperformed model based on the highest value of R-squared and lowest value of RMSE, bold adjusted *p* value indicates as statistically significant at level of 0.05

radiotherapy outcome [26]. Many studies have been conducted to find the main mechanisms of such effects induced by metformin. However, these studies are based on the invasive molecular studies that are also expensive and time consuming. Recently by introducing radiomics and studies on the correlation between imaging features and genes/proteins, it was clarified that quantitative imaging measures can be used as non-invasive, easy to use, and cost-effective biomarkers to decode the biological pathways involved in cancer diagnosis and treatment [27, 28]. In this paper, we aimed to find how CT imaging features can reveal the proteomics pathways in metformin-enhanced radiosensitivity.

In this work, we found that some proteins involved in radiosensitivity pathways have correlation with tumor volume changes. We identified that proteins, phospho-4EBP1, phospho-mTOR, and mTOR, are highly correlated to tumor volume changes in days 12 to 28. As these proteins have a great role in metformin pathways, they act as key parameters to enhance radiation cell killing and, therefore, reduce the volume size of tumor. These results could pave the way for personalized therapy using radiomics features, if confirmed by larger sample sizes in both preclinical and clinical studies. These features provide insights into the key mechanisms underlying drug-induced treatment modulation. On the other hand, by finding correlation between radiomics features and proteins, new drugs can be discovered or optimized based on the medical imaging.

In an interesting part of our study, we observed that several radiomics features have correlation to proteins in metformin-enhanced radiosensitivity pathway. We identified that feature Wavelet_HHH_firstorder_Median is highly correlated to phospho-ACC, AMPK-alpha and phospho-AMPK – alpha, Dependence_Low_Gray_Level_Emphasis is correlated to phospho-AMPK-alpha, and GLCM_Cluster

Table 2 Feature selection for identify of related features with change tumor volume (Day 28-baseline) by "glmnet" and "glmnetSE" R packages with 1000 bootstrapping and leave-one-out cross-validation and "glm" R function for calculation of *p* value and comparison of goodness of fit among groups (Control was considered as the reference)

Groups	Selected variables	Variable importance	Adj. *p* value	Adjusted R^2	*p* value of comparison between groups
Control	wavelet-HHLglcmContrast	51%	**0.043**	0.258	Reference
	wavelet-LHLglcmInverseVariance	50%	0.069		
	wavelet-LHLgldmLowGrayLevelEmphasis	39%	0.260		
	log-sigma-5–0-mm-3DglcmImc2	60%	**0.011**		
	wavelet-LHLglrlmLowGrayLevelRunEmphasis	29%	0.490		
	log-sigma-2–5-mm-3DglszmLowGrayLevelZoneEmphasis	43%	0.286		
	wavelet-HLLngtdmStrength	65%	**0.009**		
	log-sigma-4–0-mm-3DglrlmShortRunLowGrayLevelEmphasis	47%	0.243		
	log-sigma-4–5-mm-3DglszmSmallAreaLowGrayLevelEmphasis	37%	0.365		
Metformin	wavelet-HHHfirstorderUniformity	62%	**0.012**	0.399	0.003
	log-sigma-0–5-mm-3DglrlmLongRunLowGrayLevelEmphasis	77%	**0.008**		
	log-sigma-3–5-mm-3DglcmInverseVariance	93%	**0.001**		
IR	wavelet-LHLglcmInverseVariance	77%	**0.011**	0.418	0.001
	wavelet-HHLglszmSmallAreaLowGrayLevelEmphasis	71%	**0.030**		
	originalglszmSmallAreaEmphasis	84%	**0.005**		
	wavelet-LLHglcmCorrelation	95%	**0.001**		
	log-sigma-3–0-mm-3DglszmSmallAreaEmphas	55%	0.160		
	wavelet-LLLglrlmLongRunLowGrayLevelEmphasis	31%	0.456		
	wavelet-LHHglszmSizeZoneNonUniformityNormalized	27%	0.520		
IR + Metformin	log-sigma-2–0-mm-3DglcmClusterShade	98%	**< 0.001**	**0.608**	< 0.001
	wavelet-LHHglszmLowGrayLevelZoneEmphasis	86%	**0.001**		
	originalgldmSmallDependenceLowGrayLevelEmphasis	72%	**0.003**		
	wavelet-HLLgldmGrayLevelNonUniformity	66%	**0.005**		
	wavelet-LHLngtdmStrength	62%	**0.010**		
	log-sigma-5–0-mm-3DglcmDifferenceVariance	57%	**0.032**		
	wavelet-HHHfirstorderMedian	55%	**0.039**		

p value by Wald chi-square test, Adj. *p* value: *p* value adjusted by Benjamini and Hochberg method, overall R^2 is based on the multivariable linear regression, last column indicates *p* values for statistical comparisons of linear models among the groups (Control as a reference group) using likelihood ratio test (LRT), bold adjusted R-squared indicates the best outperformed model based on the highest value of R-squared and lowest value of RMSE, bold adjusted *p* value indicates as statistically significant at level of 0.05

Shade is correlated to phospho-mTOR and mTOR. As was described in previous papers [29], these features measure the distribution of pixel intensities and show how heterogeneities within a tumor could be measured by such simple parameters.

Understanding the biological meaning of radiomics is an active area of research. Several human and animal studies have attempted to address these issues. In a recent animal trial, correlations between the expression of histological tumor microenvironment (TME) and MRI radiomics features were analyzed and correlation between texture features and hypoxia biomarkers was found [30]. In a review paper [31], the biological meaning of radiomics features is discussed and it was proposed that radiomics studies should be biologically validated in the process of model building or subsequent validation. It is also having to be mentioned that biological validation of such preclinical studies is not sufficient and human trials are needed for further validation.

Several radioproteomics studies have been conducted in some types of cancer. For example, in a study by Kayadibi et al., Ki-67 expression was predicted in breast cancer using MRI radiomics features [32]. Lehrer et al. [33], investigated links between MRI features to deregulated protein expression and pathway activity in lower grade glioma using multiple-response regression analysis. They identified that multiple proteins associated with imaging features. In this study, it was observed that VASARI features have correlation with expression of IL8, PTEN, PI3K/Akt, Neuregulin, ERK/MAPK, p70S6K, and EGF signaling pathways. Beer et al. [34], investigated the association between CT features

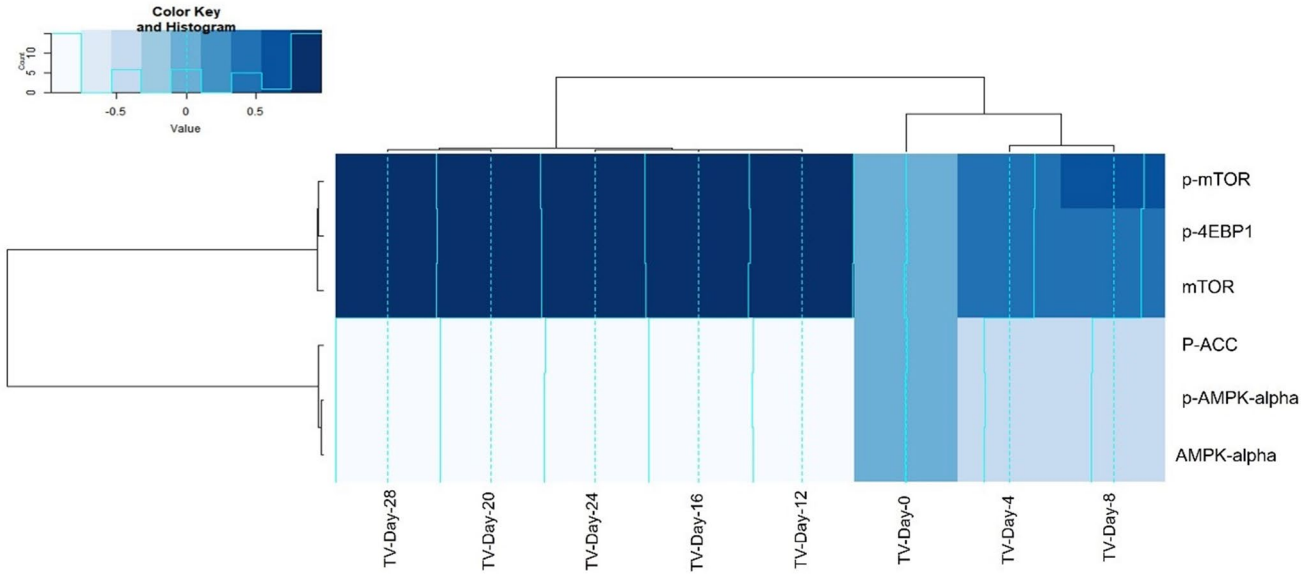

Fig. 4 Bi-cluster heatmap plot of correlations between proteins expression and tumor volume over time. *p-AMPK-alpha*: phospho-AMPK-alpha; *P-ACC*: phospho-ACC, *p-mTOR*: phospho-mTOR, *p-4EBP1*: phospho-4EBP1, *TV*: tumor volume

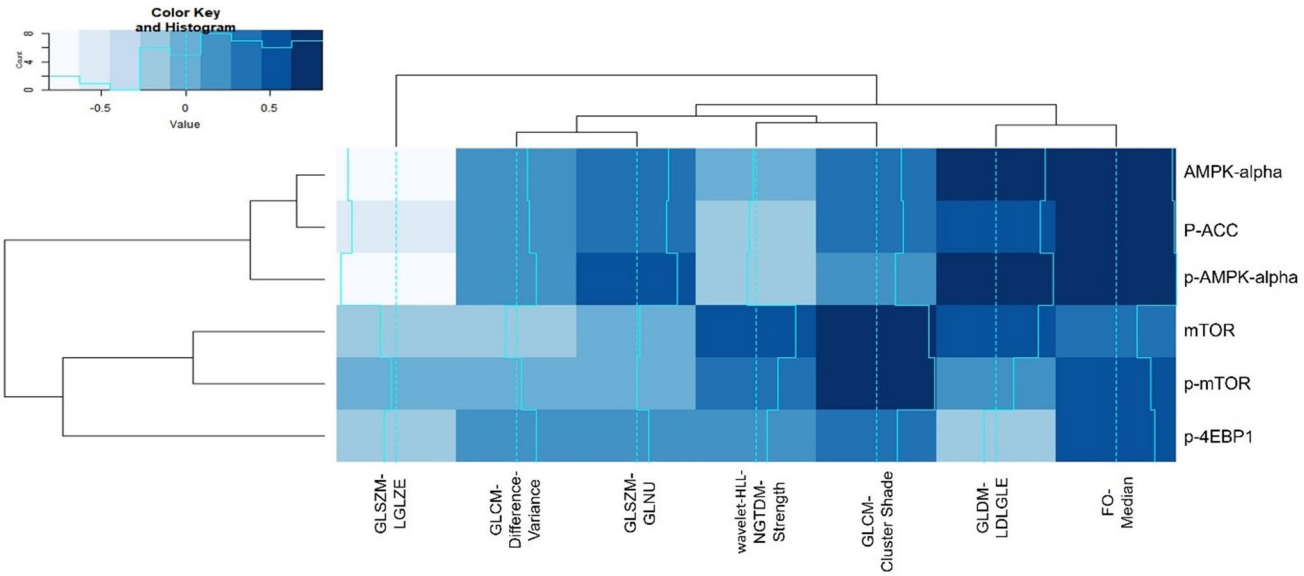

Fig. 5 Bi-cluster heatmap plot of correlations between proteins expression and related features with change tumor volume in IR plus Metformin group. *p-AMPK-alpha*: phospho-AMPK-alpha, *P-ACC*: phospho-ACC, *p-mTOR*: phospho-mTOR, *p-4EBP1*: phospho-4EBP1

with proteomic data in patients with high-grade serous ovarian cancer and observed association between the CRIP2 and CKB proteins and some texture features that represented intra- and inter-site tumor heterogeneity.

Due to the nature of using an animal model, this study has some limitations. First, a total of 8 mice per group is a small sample size for multiple testing in this study. Second, we employed a clinical CT scanner for our tests, but using micro-CT, which has a higher resolution, could enhance the quality of this study. However, Kirschner et al. [35] showed that clinical CT scanner may reliably be used for in vivo imaging and volumetric analyses of brain tumor growth in mice. Moreover, they reported that clinical CT scanner allow the in vivo detection of macroscopic changes of tumor morphology in mice. Furthermore, we recommend a quantitative assessment of the reproducibility of the selected radiomics features for future analysis. It would enhance the prediction power of the models.

Conclusion

In the present study, we identified radiomics features can decode proteins that involved in response to metformin and radiation. In this preclinical study, several CT features have been found as markers to capture biological information by a non-invasive manner. Further studies are warranted to investigate the optimal way to integrate radiomics into biological experiments.

Funding This research was financially supported by Cancer Research Center (Grant Number: CRC-9916) from the vice chancellor of research at Ahvaz Jundishapur University of Medical Sciences (Iran).

Declarations

Conflict of interest The authors declare that they have no conflict of interest.

Ethics approval All animal experiments in this study were carried out based on the NIH Guide for Care and Use of Laboratory Animals. All procedures were approved by the Committee on the Ethics of Animal Experiments of Ahvaz Jundishapur University of Medical Sciences (Approval Number: IR.AJUMS.ABHC.REC.1399.023).

References

1. Koritzinsky M. Metformin: a novel biological modifier of tumor response to radiation therapy. Int J Radiat Oncol Biol Phys. 2015;93(2):454–64.
2. Mortezaee K, Shabeeb D, Musa AE, Najafi M, Farhood B. Metformin as a radiation modifier; implications to normal tissue protection and tumor sensitization. Curr Clin Pharm. 2019;14(1):41–53.
3. Samsuri NAB, Leech M, Marignol L. Metformin and improved treatment outcomes in radiation therapy–a review. Cancer Treat Rev. 2017;55:150–62.
4. Gash K, Chambers A, Cotton D, Williams A, Thomas M. Potentiating the effects of radiotherapy in rectal cancer: the role of aspirin, statins and metformin as adjuncts to therapy. Br J Cancer. 2017;117(2):210–9.
5. Saraei P, Asadi I, Kakar MA, Moradi-Kor N. The beneficial effects of metformin on cancer prevention and therapy: a comprehensive review of recent advances. Cancer Manag Res. 2019;11:3295.
6. Chevalier B, Pasquier D, Lartigau EF, Chargari C, Schernberg A, Jannin A, et al. Metformin:(future) best friend of the radiation oncologist? Radiother Oncol. 2020;151:95–105.
7. Clifford RE, Gerrard AD, Fok M, Vimalachandran D. Metformin as a radiosensitiser for pelvic malignancy: a systematic review of the literature. Eur J Surg Oncol. 2021;47(6):1252–7.
8. Wang B, Dong J, Xiao H, Li Y, Jin Y, Cui M, et al. Metformin fights against radiation-induced early developmental toxicity. Sci Total Environ. 2020;732: 139274.
9. Cheki M, Shirazi A, Mahmoudzadeh A, Bazzaz JT, Hosseinimehr SJ. The radioprotective effect of metformin against cytotoxicity and genotoxicity induced by ionizing radiation in cultured human blood lymphocytes. Mutat Res Genet Toxicol Environ Mutagen. 2016;809:24–32.
10. Buckley AM, Lynam-Lennon N, O'Neill H, O'Sullivan J. Targeting hallmarks of cancer to enhance radiosensitivity in gastrointestinal cancers. Nat Rev Gastroenterol Hepatol. 2020;17(5):298–313.
11. Adeberg S, Bernhardt D, Harrabi SB, Nicolay NH, Hörner-Rieber J, König L, et al. Metformin enhanced radiosensitivity associates with G2/M cell cycle arrest and elevated adenosine-5'-monophosphate-activated protein kinase levels in glioblastoma. Radiol Oncol. 2017;51(4):431–7.
12. Zhang Y, Storr SJ, Johnson K, Green AR, Rakha EA, Ellis IO, et al. Involvement of metformin and AMPK in the radioresponse and prognosis of luminal versus basal-like breast cancer treated with radiotherapy. Oncotarget. 2014;5(24):12936.
13. Kimura N, Tokunaga C, Dalal S, Richardson C, Ki Y, Hara K, et al. A possible linkage between AMP-activated protein kinase (AMPK) and mammalian target of rapamycin (mTOR) signalling pathway. Genes Cells. 2003;8(1):65–79.
14. Musa J, Orth M, Dallmayer M, Baldauf M, Pardo C, Rotblat B, et al. Eukaryotic initiation factor 4E-binding protein 1 (4E-BP1): a master regulator of mRNA translation involved in tumorigenesis. Oncogene. 2016;35(36):4675–88.
15. Abdollahi H, Shiri I, Heydari M. Medical imaging technologists in radiomics era: an alice in wonderland problem. Iran J Pub Health. 2019;48(1):184.
16. Abdollahi H, Chin E, Clark HD, Hyde DE, Thomas S, Wu J, et al. Radiomics-guided radiation therapy: opportunities and challenges. Phys Med Biol. 2022;67(12):TR02.
17. Shiri I, Amini M, Nazari M, Hajianfar G, Avval AH, Abdollahi H, et al. Impact of feature harmonization on radiogenomics analysis: prediction of EGFR and KRAS mutations from non-small cell lung cancer PET/CT images. Comput Biol Med. 2022;142: 105230.
18. Shiri I, Maleki H, Hajianfar G, Abdollahi H, Ashrafinia S, Hatt M, et al. Next-generation radiogenomics sequencing for prediction of EGFR and KRAS mutation status in NSCLC patients using multimodal imaging and machine learning algorithms. Mole Imaging Biol. 2020;22(4):1132–48.
19. Becker AS, Schneider MA, Wurnig MC, Wagner M, Clavien PA, Boss A. Radiomics of liver MRI predict metastases in mice. Eur Radiol Exp. 2018;2(1):1–10.
20. Panth KM, Leijenaar RT, Carvalho S, Lieuwes NG, Yaromina A, Dubois L, et al. Is there a causal relationship between genetic changes and radiomics-based image features? An in vivo preclinical experiment with doxycycline inducible GADD34 tumor cells. Radiother Oncol. 2015;116(3):462–6.
21. Storozhuk Y, Hopmans S, Sanli T, Barron C, Tsiani E, Cutz J, et al. Metformin inhibits growth and enhances radiation response of non-small cell lung cancer (NSCLC) through ATM and AMPK. Br J Cancer. 2013;108(10):2021–32.
22. Tomayko MM, Reynolds CP. Determination of subcutaneous tumor size in athymic (nude) mice. Cancer Chemother Pharmacol. 1989;24:148–54.
23. Rohde S, Lindner T, Polei S, Stenzel J, Borufka L, Achilles S, et al. Application of in vivo imaging techniques to monitor therapeutic efficiency of PLX4720 in an experimental model of microsatellite instable colorectal cancer. Oncotarget. 2017;8(41):69756.
24. Meinshausen N, Meier L, Bühlmann P. P-values for high-dimensional regression. J Am Stat Assoc. 2009;104(488):1671–81.
25. Galili T, O'Callaghan A, Sidi J, Sievert C. heatmaply: an R package for creating interactive cluster heatmaps for online publishing. Bioinformatics. 2018;34(9):1600–2.
26. Agbele AT, Faromika OP, Awe OO, Amodu FR, Edaogbogun GO, Bello KA. Impact of metformin on the therapeutic effect of radiotherapy. Radiat Med Protect. 2021;2(01):17–22.
27. Abdollahi H, Tanha K, Mofid B, Razzaghdoust A, Saadipoor A, Khalafi L, et al. MRI radiomic analysis of IMRT-induced

bladder wall changes in prostate cancer patients: a relationship with radiation dose and toxicity. J Med Imaging Radiat Sci. 2019;50(2):252–60.
28. Abdollahi H, Mahdavi SR, Shiri I, Mofid B, Bakhshandeh M, Rahmani K. Magnetic resonance imaging radiomic feature analysis of radiation-induced femoral head changes in prostate cancer radiotherapy. J Cancer Res Ther. 2019;15(8):S11–9.
29. Ardakani AA, Bureau NJ, Ciaccio EJ, Acharya UR. Interpretation of radiomics features: a pictorial review. Comput Meth Program Biomed. 2021;215:106609. https://doi.org/10.1016/j.cmpb.2021.106609.
30. Müller J, Leger S, Zwanenburg A, Suckert T, Lühr A, Beyreuther E, et al. Radiomics-based tumor phenotype determination based on medical imaging and tumor microenvironment in a preclinical setting. Radiother Oncol. 2022;169:96–104.
31. Tomaszewski MR, Gillies RJ. The biological meaning of radiomic features. Radiology. 2021;298(3):505–16.
32. Kayadibi Y, Kocak B, Ucar N, Akan YN, Akbas P, Bektas S. Radioproteomics in breast cancer: prediction of Ki-67 expression with MRI-based radiomic models. Acad Radiol. 2022;29:S116–25.
33. Lehrer M, Bhadra A, Aithala S, Ravikumar V, Zheng Y, Dogan B, et al. High-dimensional regression analysis links magnetic resonance imaging features and protein expression and signaling pathway alterations in breast invasive carcinoma. Oncoscience. 2018;5(1–2):39.
34. Beer L, Sahin H, Bateman NW, Blazic I, Vargas HA, Veeraraghavan H, et al. Integration of proteomics with CT-based qualitative and radiomic features in high-grade serous ovarian cancer patients: an exploratory analysis. Euro Radiol. 2020;30(8):4306–16.
35. Kirschner S, Mürle B, Felix M, Arns A, Groden C, Wenz F, et al. Imaging of orthotopic glioblastoma xenografts in mice using a clinical CT scanner: comparison with micro-CT and histology. PLoS ONE. 2016;11(11): e0165994.